A Triple-Band Triple-Polarization Endfire/Broadside Millimeter-Wave Phased Array Cavity Antenna With Small Frequency Ratio

Zhonghe Zhang, *Student Member, IEEE*, Sai-Wai Wong, *Senior Member, IEEE*, Ruisen Chen, *Member, IEEE*, Shu-Qing Zhang, *Student Member, IEEE*, Guanlong Huang, *Senior Member, IEEE*, and Yejun He, *Senior Member, IEEE*

***Abstract*—A phased array of triple-mode cavity antennas (TMCA) has been developed and designed for multiband millimeter-wave (mmWave) applications. It dynamically adjusts frequency to simultaneously change polarization and beam direction, while also adapting broadside and endfire directions. The unique design of the cavity mode results in small frequency ratios, 1.033 and 1.025. The 1 × 4 TMCA achieves a peak gain of 12 dBi in the endfire direction for vertical polarization (VP) radiation, while obtaining peak gains of 13.6 dBi for horizontal polarization (HP) radiation and 13 dBi for vertical polarization (VP) radiation in the broadside direction. The three radiation beam coverages can achieve gains exceeding 9 dBi within a scanning range of 60 °. The TMCA presents low complexity, high gain, support for orthogonal polarization, and the dual capability of endfire or broadside beam coverage, rendering it suitable for mm-Wave communication in both base stations and vehicular applications.**

***Index Terms*—Millimeter-wave, small frequency ratio, tripleband, triple-mode cavity antenna (TMCA), triple-polarization.**

I. Introduction

THE swift advancement of fifth-generation (5G) cellular network technology is leveraging the millimeter-wave (mmWave) frequency range to offer unmatched data capacity and communication speed for mobile devices [1], [2], [3], [4], [5], [6], [7], [8]. The mmWave spectrum boasts higher absolute bandwidth but lower relative bandwidth. To enhance millimeter-wave spectrum utilization, improve beam coverage, and reduce polarization loss factors, research on multifrequency, multipolarization, and multibeam coverage for mmWave antennas is becoming increasingly crucial.

Manuscript received 16 January 2024; accepted 1 February 2024. Date of publication 14 February 2024; date of current version 4 December 2024. This work was supported in part by the National Key Research and Development Program of China under Grant 2023YFE0107900 and in part by the National Natural Science Foundation of China under Grant 62071306. *(Corresponding author: Sai-Wai Wong.)*

Zhonghe Zhang, Sai-Wai Wong, Shu-Qing Zhang, and Yejun He are with the State Key Laboratory of Radio Frequency Heterogeneous Integration, Sino-British Antennas and Propagation Joint Laboratory, Guandong Engineering Research Center of Base Station Antennas and Propagation, Shenzhen Key Laboratory of Antennas and Propagation, College of Electronics and Information Engineering, Shenzhen University, Shenzhen 518060, China (e-mail: 422384683@qq.com; wongsaiwai@ieee.org; 2100432054@email.szu.edu.cn; heyejun@126.com).

Ruisen Chen and Guanlong Huang are with the School of AI-Guangdong, Foshan University, Foshan 528225, China (e-mail: crs@fosu.edu.cn; hgl@fosu.edu.cn).

Digital Object Identifier 10.1109/LAWP.2024.3362817

Several methods exist for achieving multiband capabilities, including shared aperture slot antenna arrays [9], surface plasmon resonance antennas [10], patch antennas [11], [12], and cavity slot antennas [13], [14]. To enhance frequency coverage while reducing polarization loss factors, multifrequency antennas with orthogonal polarizations have been proposed. These improvements are achieved either through modified feeding networks [15] or by utilizing characteristic mode analysis [16] to achieve orthogonal dual-polarization. Tuning different mode frequencies for a small frequency ratio dual circular polarization has also been adopted [17], [18], [19]. Additionally, [20] introduced a counterintuitive beamforming technique in two bands. The frequency ratios of the aforementioned multiband antennas are all higher than 1.04, and they are not designed specifically for mmWave applications. At [21], the mmWave generates three different polarization states: right-hand circular polarization (RHCP), linear polarization (LP), and left-hand circular polarization (LHCP).

In this letter, a triple-band, triple-polarization endfire /broadside mmWave phased array is presented. The antenna array adopts a triple-mode cavity resonator and a single feed mode. The design aims to excite three fundamental modes, TE_{011}, TE_{101}, and TM_{110}, within the metal cavity. The primary contributions of the letter to the authors' best knowledge are as follows.

1) Allocation of the three fundamental modes across three contiguous frequency bands accomplishes a small frequency ratio of 1.03 and 1.025, which is the smallest in literature.
2) Three orthogonal polarization radiation beams in two directions have never been reported in the literature.
3) Orthogonal polarization is produced in the broadside direction and vertical polarization in the endfire direction, a concept yet to be proposed in multifrequency antennas with three beams scanning ability.

The final 1×4 triple-mode cavity antenna (TMCA) is designed to operate across triple bands: 26.76, 27.65, and 28.44 GHz.

II. Antenna Design

A. TMCA Design

The metal cavity resonator antenna depicted in Fig. 1 has external dimensions a, b, and c, and internal dimensions a_1, b_1, and c_1. Three different modes are excited through rotation and

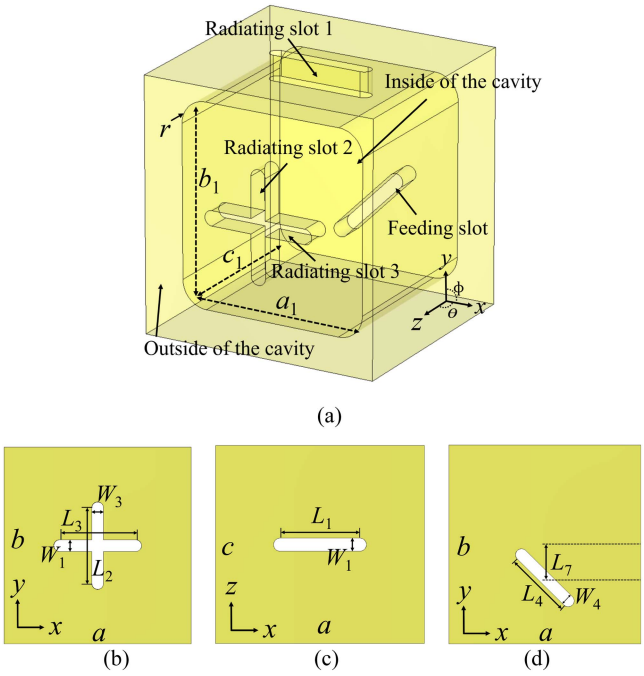

Fig. 1. Proposed triple-mode cavity antenna. (a) 3-D view. (b) Top view. (c) Side view. (d) Bottom view. Dimensions (Unit: mm): $a = 9.6$, $b = 10.1$, $c = 9.1$, $a_1 = 7.6$. $b_1 = 8.1$, $c_1 = 7.1$, $L_1 = 3.67$, $W_1 = 0.6$, $L_2 = 3.89$, $W_2 = 0.6$, $L_3 = 3.91$. $W_3 = 0.6$, $L_4 = 3.3$, $W_4 = 0.6$.

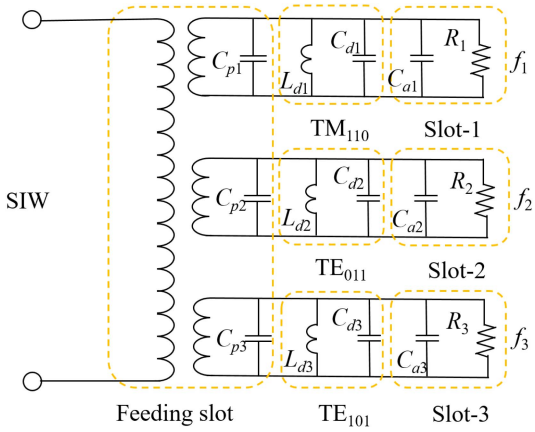

Fig. 2. Equivalent circuit model of the proposed antenna.

biasing of the feeding slot. Radiating slot 1 on the side has a length of L_1 and a width of W_1, designed for achieving endfire horizontal polarization. Meanwhile, mutually perpendicular radiating slots 2 and 3 have lengths L_2 and L_3, and widths W_1 and W_2, respectively, intended for achieving broadside horizontal and vertical polarizations. The bottom features a feeding slot with a length and width of L_4 and W_4.

The antenna's equivalent circuit is illustrated in Fig. 2, wherein C_{p1}, C_{p2}, and C_{p3}, respectively denote the capacitive loads of individual feedings in different modes. Additionally, C_{a1}, C_{a2}, and C_{a3} represent the capacitive loads of radiating slots in distinct modes. (L_{d1}, C_{d1}), (L_{d2}, C_{d2}), and (L_{d3}, C_{d3}) represent the resonator models for the TM_{110} mode, TE_{011} mode, and TE_{101} mode. The resonant frequencies of the three resonance modes [22] can be calculated using the following formulas as a result of the extremely small frequency ratios

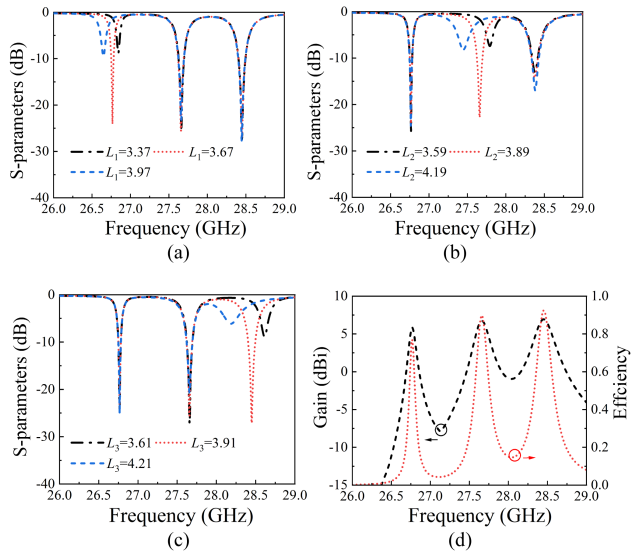

Fig. 3. Influence of the regulating radiation slot on frequency. (a) Versus length L_1. (b) Versus length L_2. (c) Versus length L_3. Dimensional unit: mm. (d) gain and efficiency of TMCA.

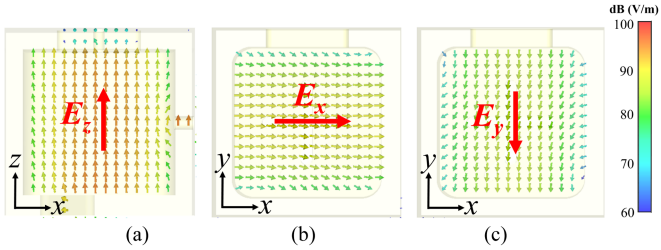

Fig. 4. Electric field distributions. (a) Electric field TM_{110} mode, f_1. (b) Electric field TE_{011} mode, f_2. (c) Electric field TE_{101} mode, f_3.

introduced by the metallic cavity structure:

$$f_1 = \frac{1}{2\pi\sqrt{L_{d1}\left(C_{p1} + C_{d1} + C_{a1}\right)}} \tag{1}$$

$$f_2 = \frac{1}{2\pi\sqrt{L_{d2}\left(C_{p2} + C_{d2} + C_{a2}\right)}} \tag{2}$$

$$f_3 = \frac{1}{2\pi\sqrt{L_{d3}\left(C_{p3} + C_{d3} + C_{a3}\right)}}. \tag{3}$$

Fig. 3(a)–(c) shows the influence of the regulating radiation slot on frequency. The frequency control of each radiator is individual, which makes it possible for three beam controls with different properties. In Fig. 3(d), the TMCA's gain and efficiency are displayed. The characteristics and orientations of the beams at the three frequencies are not consistent. The three frequencies of this cavity are designed at 26.76, 27.65, and 28.44 GHz. The small frequency ratio allows the antenna to achieve different polarizations within the 5G mmWave range while maintaining performance for both endfire and broadside radiating antennas.

Fig. 4 depicts electric fields orthogonal in three directions and at three frequencies. Although TM_{110} and TE_{101} modes generate the same vertical polarization, they are distributed in different directions, covering wide beam scanning in both endfire and broadside directions.

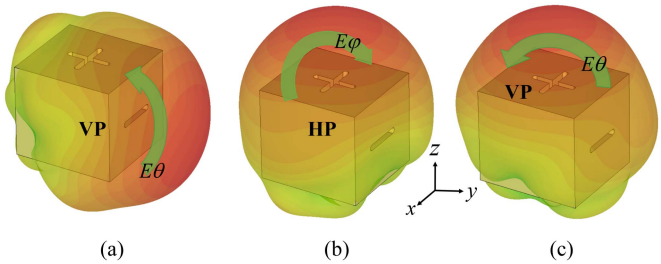

Fig. 5. Simulates the radiation pattern in three frequency bands. (a) f_1. (b) f_2. (c) f_3.

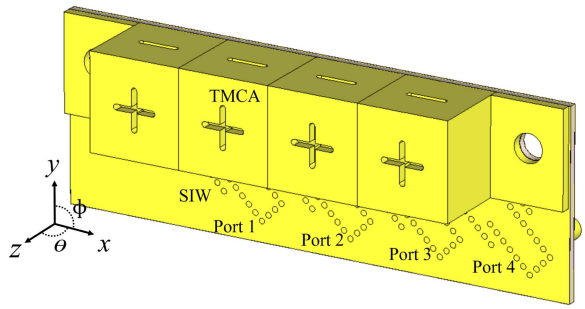

Fig. 6. 1×4 phased array architecture of TMCA with four ports.

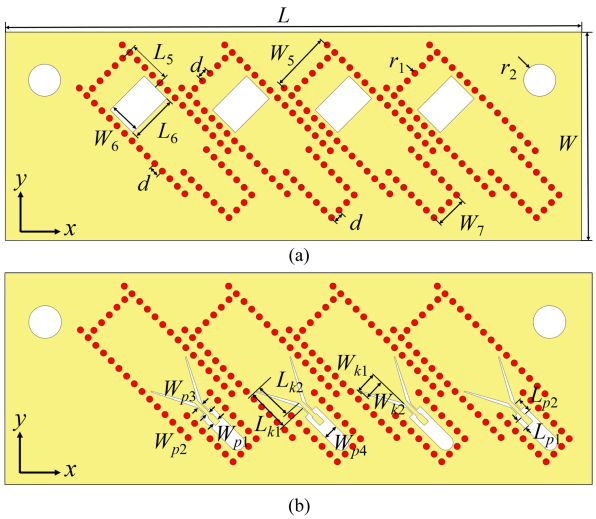

Fig. 7. Feed substrate of TMCA antenna array. (a) Top view. (b) Bottom view. Dimensions (Unit: mm): $d = 1$, $r_1 = 0.3$, $r_2 = 1.5$, $L_5 = 4.1$, $W_5 = 5.7$, $L_6 = 4.5$, $W_6 = 3$, $L_7 = 1.7$, $W_7 = 3$, $L_{k1} = 4.1$, $L_{k2} = 3.6$, $W_{k1} = 2.3$, $W_{k2} = 2.2$, $L_{p1} = 1$, $L_{p2} = 1.3$, $W_{p1} = 0.55$, $W_{p2} = 0.35$, $W_{p3} = 0.55$, $W_{p4} = 1.4$.

Fig. 5 illustrates radiation patterns for these three frequencies, with the green arrows indicating the direction of the electric field. This demonstrates diverse polarizations while ensuring balanced antenna radiation with both broadside and endfire components

B. 1×4 TMCA Phased Array Design

To prevent mutual interference of RF signals and enhance system integration, the design incorporates Mini Subminiature Push-On (Mini-SMP) connector waveguide transitions, followed by transitioning to substrate-integrated waveguides (SIWs) for feeding the triple mode cavity antenna.

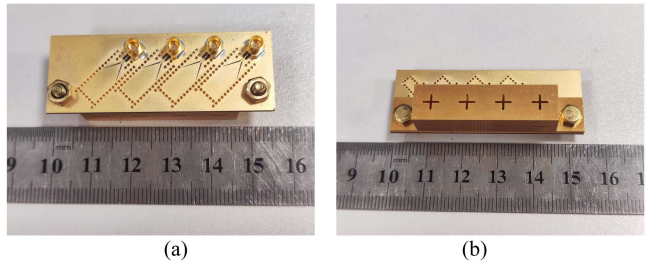

Fig. 8. Photograph of the fabricated prototype. (a) Top view. (b) Bottom view.

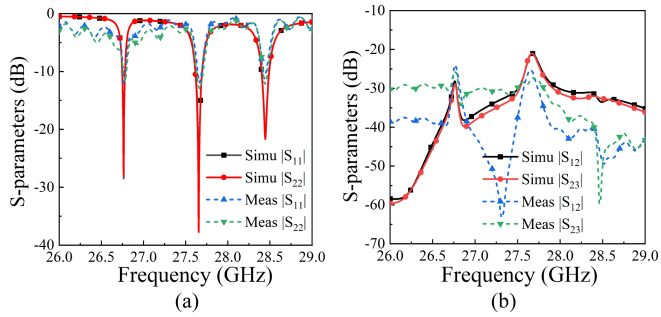

Fig. 9. (a) Simulated and measured return loss for ports 1 and 2. (b) Simulated and measured between nearby ports.

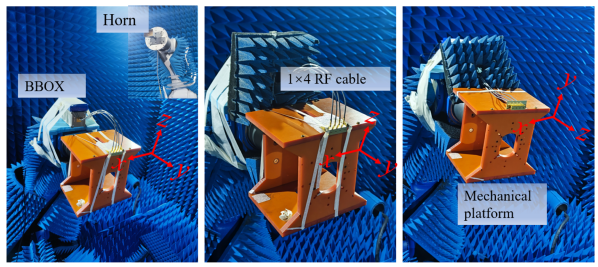

Fig. 10. Far-field measurement setup of 1×4 active phased array module of the TMCA.

TABLE I
BEAM SCANNING RANGE IN BROADSIDE/ENDFIRE

Fre./Propag.	Pol.	Realized Gain (dBi)				Scanning angle
		0	10	20	25	
26.76/+y	VP	12	11.6	11.2	10.5	34
27.65/+z	HP	13.6	10.4	9.79	9.53	33
28.44/+z	VP	13	12.5	12	11.7	31

The complete antenna structure is illustrated in Fig. 6, comprising a 4-element antenna array distributed along the x-axis. The antenna is divided into two sections, consisting of a 1×4 TMCA and a feeding substrate. The 1×4 TMCA is crafted using computer numerical control (CNC) metal machining and connected to the feed substrate with screws. The SIW feed channel is inclined to 45°. The antenna substrate in Fig. 7 is made of Rogers5880 material with a thickness of 0.787 mm and a dielectric constant of 2.2. Four surface mount Mini-SMPs will be soldered at the position from Port1 to Port4. The detailed dimensions of the feeding substrate have been optimized with CST.

TABLE II
COMPARISONS WITH REPORTED SMALL FREQUENCY RATIO ANTENNAS

Ref.	Configuration	Frequency band (GHz)	Frequency ratio	Beam direction	Polarization
[10]	Surface plasmon	10.2/10.78/9.7/10.75/4.8/7.08	1.06-1.5	End-fire	Linear
[20]	2×4 array	5/5.8	1.16	Broadside	Linear
[15]	Patch	1.25 /2.10	1.6-3.5	Broadside	Linear orthogonal
[16]	Patch	1.655 /2.370	1.057-1.706	Broadside	Linear orthogonal
[13]	Cavity	2.97/3.18	1.07	Broadside	Linear orthogonal
[17]	Patch	2.134/2.223	1.04	Broadside	RHCP LHCP
[18]	Slot	1.88/2.39	1.27	Broadside	RHCP LHCP
[21]	SIW cavity	28/33/38/	1.18/1.15	Broadside	RHCP LP LHCP
This work	Cavity	26.76/27.65/28.44	1.033/1.025	End-fire/Broadside	VP (End-fire) Linear orthogonal (Broadside)

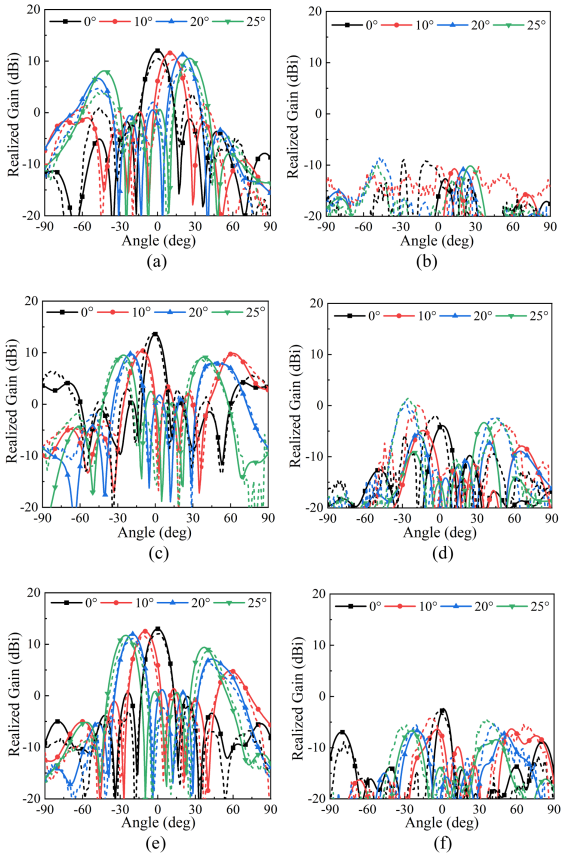

Fig. 11. Simulated and measured beam scanning radiation patterns (solid: simulation, dashed: measurement). (a) Co-pol endfire at 26.76 GHz endfire. (b) Cross-pol endfire at 26.76 GHz. (c) Co-pol of broadside at 27.65 GHz. (d) Cross-pol of broadside at 27.65 GHz. (e) Co-pol of broadside at 28.44 GHz. (f) Cross-pol of broadside at 28.44 GHz.

III. ANTENNA ARRAY FABRICATION AND MEASUREMENTS

To validate the proposed 1×4 single-feed triple-band triple-polarization millimeter-wave phased array, a prototype is fabricated, as depicted in Fig. 8.

The simulation and measurement of the antenna return loss are illustrated in Fig. 9. Due to symmetry considerations, only the return loss of Port1 and Port2 is displayed. The $|S_{11}|$ of the three frequencies, 26.76, 27.65, and 28.44 GHz, are all below −10 dB. The presence of ripples is a result of multipath interference during the welding and testing processes. The measured results align with the simulation outcomes. The simulation and measurement of antenna isolation are illustrated in Fig. 9(b). Due to the inherent characteristics of the cavity and the substantial spacing between feed sources, the isolation between Port1 and Port2, as well as between Port2 and Port3, at frequencies 26.76, 27.65, and 28.44 GHz, is all below −15 dB. The measured results are consistent with the simulation results.

To validate the beam-steering capabilities of the multimode metallic phased array cavity antenna, constructing a far-field measurement environment, as shown in Fig. 10. Fig. 11 presents radiation pattern plots at scan angles of 0°, 10°, 20°, and 25°, show casing distinct polarization characteristics in different directions. Test results closely match simulation results, with an error within 1.5 dBi. Achieving high gain and beam scanning with gains exceeding 9 dBi at angles above 50°. As the scanning angles are symmetric, only half of the antenna beams' scan effects are displayed for clarity. Specific experimental data is provided in Table I.

Compared to the multiband antenna in Table II, TMCA achieves a small frequency ratio of 1.033/1.025 due to the high-Q resonance characteristics of the cavity, offering both broadside orthogonal polarization and endfire beam coverage.

IV. CONCLUSION

This letter presents a novel approach involving a metal cavity antenna that utilizes resonance in three modes. This innovative design enables the sequential excitation of vertical polarization in the endfire direction, followed by orthogonal linear polarization in the broadside direction, all while achieving effective multi-band operation. To validate this, a phased-array antenna operating in the mmWave frequency range is constructed based on the proposed design concept, and measurements are conducted to confirm the effectiveness of the introduced design. In conclusion, the TMCA demonstrates attributes such as a small frequency ratio, multidimensional triple-polarization radiation capabilities and versatile adaptability to diverse prescribed frequencies.

REFERENCES

[1] W. Hong et al., "Multibeam antenna technologies for 5G wireless communications," *IEEE Trans. Antennas Propag.*, vol. 65, no. 12, pp. 6231–6249, Dec. 2017.

[2] T. S. Rappaport, Y. Xing, G. R. MacCartney, A. F. Molisch, E. Mellios, and J. Zhang, "Overview of millimeter wave communications for fifth-generation (5G) wireless networks—With a focus on propagation models," *IEEE Trans. Antennas Propag.*, vol. 65, no. 12, pp. 6213–6230, Dec. 2017.

[3] J. G. Andrews et al., "What will 5G be?," *IEEE J. Sel. Areas Commun.*, vol. 32, no. 6, pp. 1065–1082, Jun. 2014.

[4] H. Ullah, N. Gopalakrishnan Nair, A. Moore, C. Nugent, P. Muschamp, and M. Cuevas, "5G communication: An overview of vehicle-to-everything, drones, and healthcare use-cases," *IEEE Access*, vol. 7, pp. 37251–37268, 2019.

[5] Y. Zeng, Q. Wu, and R. Zhang, "Accessing from the sky: A tutorial on UAV communications for 5G and beyond," *Proc. IEEE*, vol. 107, no. 12, pp. 2327–2375, Dec. 2019.

[6] M. Colella, S. Di Meo, M. Liberti, M. Pasian, and F. Apollonio, "Advantages and disadvantages of computational dosimetry strategies in the low mmW range: Comparison between multilayer slab and anthropomorphic models," *IEEE Trans. Microw. Theory Techn.*, vol. 71, no. 10, pp. 4533–4545, Oct. 2023.

[7] X. Yang, L. Ge, Y. Ji, X. Zeng, and K. M. Luk, "Design of low-profile multiband half-mode substrate-integrated waveguide antennas," *IEEE Trans. Antennas Propag.*, vol. 67, no. 10, pp. 6639–6644, Oct. 2019.

[8] Y. Li et al., "3-D printed high-gain wideband waveguide fed horn antenna arrays for millimeter-wave applications," *IEEE Trans. Antennas Propag.*, vol. 67, no. 5, pp. 2868–2877, May 2019.

[9] D. Yang, F. Cao, and J. Pan, "A single-layer dual-frequency shared-aperture SIW slot antenna array with a small frequency ratio," *IEEE Antennas Wireless Propag. Lett.*, vol. 17, no. 6, pp. 1048–1051, Jun. 2018.

[10] H. Zhao, J. Li, Q. Zhang, S. Li, and X. Yin, "Spoof surface plasmon polariton antenna with dual-band endfire gain and flexible small frequency ratio," *IEEE Trans. Antennas Propag.*, vol. 70, no. 11, pp. 11079–11084, Nov. 2022.

[11] Y. A. Kamel, H. A. Mohamed, H. ELsadek, and H. M. ELhennawy, "Miniaturized triple-band circular-polarized implantable patch antenna for bio-telemetry applications," *IEEE Antennas Wireless Propag. Lett.*, vol. 22, no. 1, pp. 74–78, Jan. 2022.

[12] H. Zhai, Z. Ma, Y. Han, and C. Liang, "A compact printed antenna for triple-band WLAN/WiMAX applications," *IEEE Antennas Wireless Propag. Lett.*, vol. 12, pp. 65–68, 2013.

[13] J. Y. Lin et al., "A dual-functional triple-mode cavity resonator with the integration of filters and antennas," *IEEE Trans. Antennas Propag.*, vol. 66, no. 5, pp. 2589–2593, May 2018.

[14] J. Y. Lin, Y. Yang, S. W. Wong, X. Li, L. Wang, and E. Dutkiewicz, "Two-way waveguide diplexer and its application to diplexing in-band full-duplex antenna," *IEEE Trans. Microw. Theory Techn.*, vol. 71, no. 3, pp. 1171–1179, Mar. 2022.

[15] J. Eichler, P. Hazdra, M. Capek, T. Korinek, and P. Hamouz, "Design of a dual-band orthogonally polarized L-probe-fed fractal patch antenna using modal methods," *IEEE Antennas Wireless Propag. Lett.*, vol. 10, pp. 1389–1392, 2011.

[16] D. Fazal and Q. U. Khan, "Dual-band dual-polarized patch antenna using characteristic mode analysis," *IEEE Trans. Antennas Propag.*, vol. 70, no. 3, pp. 2271–2276, Mar. 2022.

[17] N. W. Liu, L. Zhu, Z. X. Liu, Z. Y. Zhang, and G. Fu, "Frequency-ratio reduction of a low-profile dual-band dual-circularly polarized patch antenna under triple resonance," *IEEE Antennas Wireless Propag. Lett.*, vol. 19, no. 10, pp. 1689–1693, Oct. 2020.

[18] Y. Xu, L. Zhu, N. W. Liu, and M. Li, "A dual-band dual-circularly-polarized slot antenna with stable in-band gain and reduced frequency ratio under triple resonance," *IEEE Trans. Antennas Propag.*, vol. 70, no. 11, pp. 10199–10206, Nov. 2022.

[19] Q. S. Wu, X. Zhang, L. Zhu, J. Wang, G. Zhang, and C. B. Guo, "A single-layer dual-band dual-sense circularly polarized patch antenna array with small frequency ratio," *IEEE Trans. Antennas Propag.*, vol. 70, no. 4, pp. 2668–2675, Apr. 2022.

[20] M. Li, L. Pu, M. C. Tang, and L. Zhu, "A single-layer dual-band array at low-frequency ratio with concurrent broad fan beam and narrow pencil beam," *IEEE Trans. Antennas Propag.*, vol. 70, no. 5, pp. 3354–3365, May 2022.

[21] H. Chen, Y. Shao, Y. Zhang, C. Zhang, and Z. Zhang, "A millimeter-wave triple-band SIW antenna with dual-sense circular polarization," *IEEE Trans. Antennas Propag.*, vol. 68, no. 12, pp. 8162–8167, Dec. 2020.

[22] R. S. Chen et al., "High-isolation in-band full-duplex cavity-backed slot antennas in a single resonant cavity," *IEEE Trans. Antennas Propag.*, vol. 69, no. 11, pp. 7092–7102, Nov. 2021.